ENCIT2026
21st Brazilian Congress of Thermal Sciences and Engineering

ABCM 50 ANOS
Associação Brasileira de Engenharia e Ciências Mecânicas

21st Brazilian Congress of Thermal Sciences and Engineering
November 8th-12th, 2026, Santos – SP - Brazil

# CIT26-0007
# LARGE-EDDY SIMULATION OF PREMIXED HYDROGEN-AIR FLAME PROPAGATION IN A CLOSED RECTANGULAR DUCT

**Raphael de Freitas Espíndola**
**Andrés Armando Mendiburu Zevallos**
Universidade Federal do Rio Grande do Sul
raphael.f.espindola@gmail.com
andresmendiburu@ufrgs.br

***Abstract.*** *This study presents a numerical investigation of premixed hydrogen-air flame propagation in a closed rectangular duct, using Large-Eddy Simulation (LES) with the Smagorinsky-Lilly subgrid-scale model implemented in ANSYS Fluent. The three-dimensional geometry was discretized with a structured hexahedral mesh of approximately $1\times10^6$ cells, balancing computational cost and solution accuracy. A one-step global Arrhenius kinetics mechanism calibrated for stoichiometric conditions was employed to describe hydrogen combustion. Model validation was performed through qualitative and quantitative comparison with experimental data from Jiang et al. (2024), extracting the flame-front position from the T = 1000 K isosurface and monitoring the pressure history at a fixed internal probe. A mesh sensitivity study encompassing 250,000, 500,000, and 1,000,000 elements were carried out. The validated model reproduces the characteristic flame morphologies observed experimentally, including the finger-shaped flame, the tulip flame, and the distorted tulip flame, and yields satisfactory quantitative agreement in the intermediate and late stages of propagation. The results confirm that the LES with the Smagorinsky-Lilly subgrid closure is capable of accurately capturing the dynamics of confined premixed combustion, providing a validated baseline for future investigations involving geometric obstructions.*

***Keywords:*** *confined combustion; hydrogen–air premixed flames; Large-Eddy Simulation (LES); Smagorinsky-Lilly subgrid-scale model; flame acceleration.*

## 1. INTRODUCTION

Combustion remains one of the most significant energy conversion processes in modern engineering, underpinning applications ranging from industrial energy systems and aerospace propulsion to the transport of gaseous fuels through pipeline networks. As a physico-chemical phenomenon in which chemical energy is converted into thermal and mechanical energy (Turns, 2013), it continues to drive technological development across multiple sectors. However, growing concerns over safety, efficiency, and environmental sustainability have motivated extensive research into combustion systems operating under confined conditions, where the dynamics of flame propagation are fundamentally different from open-space combustion.

Confined combustion, particularly in closed ducts, exhibits a rich array of fluid-dynamic and thermochemical phenomena that arise from the interaction between a propagating flame front and the surrounding geometry. Unlike freely propagating laminar flames, flames in confined environments accelerate due to the volumetric expansion of combustion products, the development of wall boundary layers, and the formation of hydrodynamic instabilities. Under certain conditions, this progressive acceleration can lead to the onset of the Deflagration-to-Detonation Transition (DDT), a phenomenon of critical importance both from a safety perspective and from an engineering standpoint, with potential applications in pulse detonation engines and advanced propulsion systems (Emami et al., 2015).

Among the various combustible mixtures relevant to these investigations, hydrogen-air stands out due to its exceptional properties. Hydrogen exhibits a wide flammability range (4–75% vol. in air), a high laminar burning velocity, and a low ignition energy, making hydrogen-air mixtures particularly susceptible to flame acceleration and DDT. The growing interest in hydrogen as a clean energy carrier (given that its combustion produces no carbon dioxide emissions) has further intensified the demand for a deeper understanding of its reactive flow behavior in confined geometries (Emami et al., 2015). Ensuring the safe storage, transport, and utilization of hydrogen requires a thorough characterization of how premixed hydrogen-air flames propagate and interact with geometric constraints.

From a numerical modeling perspective, the simulation of reactive flows in closed ducts presents considerable challenges. The governing equations are highly nonlinear and involve strong coupling between compressible fluid dynamics, chemical kinetics, turbulence, and heat transfer. Reynolds-Averaged Navier-Stokes (RANS) approaches have been reported to significantly overpredict flame-front velocities in confined reactive flows (Nguyen et al., 2021), owing to their inability to correctly capture near-wall turbulence dynamics and flame wrinkling mechanisms. Large-Eddy

Simulation (LES), by contrast, resolves the energy-containing turbulent scales explicitly and relies on subgrid-scale (SGS) models only for the dissipative small-scale motions, offering a substantially more faithful representation of the complex turbulence-flame interactions governing confined premixed combustion (Chen et al., 2016; Johansen and Ciccarelli, 2010).

An important aspect of confined premixed flame propagation is the emergence of characteristic flame morphologies as the flame evolves within the duct. Starting from an approximately hemispherical shape following ignition, the flame progressively adopts a finger-shaped structure driven by the elongation induced by wall boundary layers. As the flame interacts with the acoustic field established within the closed domain, pressure waves reflected from the end wall interact with the flame front, leading to the inversion of the flame curvature and the formation of the well-known tulip flame morphology. Further evolution produces the distorted tulip flame, whose intricate structure reflects the combined action of Landau-Darrieus, Rayleigh-Taylor, and Kelvin-Helmholtz hydrodynamic instabilities (Ciccarelli and Dorofeev, 2008). These morphological transitions and their governing instability mechanisms have remained an active subject of investigation, with recent numerical and experimental studies clarifying the role of flame instabilities and three-dimensional effects in the formation of the distorted tulip flame (Lei et al., 2025; Fan et al., 2026). Capturing these morphological sequences accurately is a critical benchmark for validating numerical models of confined premixed combustion.

The experimental and numerical study conducted by Jiang et al. (2024) provides a comprehensive dataset for premixed hydrogen-air flame propagation in a closed rectangular duct, serving as the primary reference for the validation of the numerical model developed in the present work. Despite the growing body of literature on confined premixed combustion (Chen et al., 2016; Karanam et al., 2018; Mei et al., 2022; Sheng et al., 2023; Wang et al., 2022), establishing a rigorously validated three-dimensional LES baseline model for the obstacle-free configuration is an essential prerequisite before extending the analysis to more complex geometries.

In this context, the present work aims to validate a three-dimensional LES computational model for premixed hydrogen-air flame propagation in a closed rectangular duct without obstacles. The numerical framework employs the Smagorinsky-Lilly SGS model and a one-step global Arrhenius kinetics mechanism within ANSYS Fluent. Validation is performed through qualitative comparison of flame morphologies and quantitative comparison of flame-front position and pressure time histories against the experimental data of Jiang et al. (2024). The validated model constitutes the foundation for subsequent investigations of obstacle-induced flame acceleration.

## 2. METHODOLOGY

### 2.1 Physical Problem and Geometry

The physical domain consists of a closed rectangular duct filled with a stoichiometric premixed hydrogen-air mixture at atmospheric conditions. The geometry was modeled in three dimensions using the Solid Edge software and exported in STEP format for importation into the ANSYS meshing environment. The duct dimensions were selected to match the experimental setup of Jiang et al. (2024), enabling direct qualitative and quantitative validation of the numerical predictions.

The duct has a rectangular cross-section and is fully closed at both ends. Ignition is initiated by a spark located at 47 mm from one of the faces, at coordinates (0.047; 0.025; 0.000) m. To reduce computational cost while preserving three-dimensional accuracy, a symmetry plane was applied along the duct mid-plane, halving the mesh size.

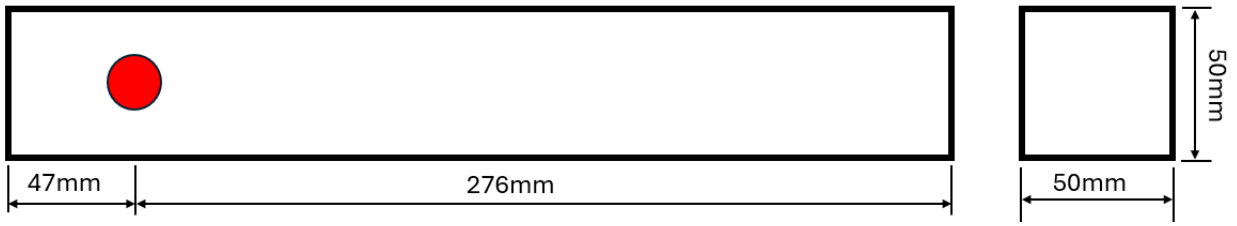


Figure 1. Duct geometry

### 2.2 Governing Equations

The numerical model is based on the Large-Eddy Simulation (LES) framework, in which the large turbulent structures are resolved directly by spatially filtering the governing equations, while the effects of the unresolved subgrid-scale (SGS) motions are modeled through an eddy-viscosity closure. The filtered conservation equations for mass, momentum, energy, and species transport were solved using the pressure-based coupled solver available in ANSYS Fluent, which is well-suited for transient, compressible, and reactive flows.

The filtered mass conservation equation is written as:

$$\frac{\partial \bar{\rho}}{\partial t} + \frac{\partial (\bar{\rho}\widetilde{u_i})}{\partial x_i} = 0 \quad (1)$$

being ρ denotes density, t, time, x, space, and $\tilde{u}_i$ are the Favre-filtered velocity components. The filtered momentum equation (Navier-Stokes) includes a subgrid-scale stress tensor $\tau_{ij}^{sgs}$ that accounts for the contribution of unresolved scales:

$$\frac{\partial (\bar{\rho}\widetilde{u_i})}{\partial t} + \frac{\partial \left(\bar{\rho}\widetilde{u_i}\widetilde{u_j} + \bar{p}\delta_{ij} - \tilde{\tau}_{ij} + \tau_{ij}^{sgs}\right)\bar{\rho}}{\partial x_j} = 0 \quad (2)$$

being $\bar{p}$ is the filtered pressure, $\tilde{\tau}_{ij}$ is the resolved viscous stress tensor, and $\tau_{ij}^{sgs}$ is the subgrid-scale (SGS) stress tensor that accounts for the momentum transport by unresolved eddies.

Conservation of total energy:

$$\frac{\partial}{\partial t}\left(\rho\left(e + \frac{v^2}{2}\right)\right) + \nabla \cdot \left(\rho v\left(h + \frac{v^2}{2}\right)\right) = \nabla \cdot \left(k_{eff}\nabla T - \sum_i h_j \vec{J}_j + \bar{\tau}_{eff} \cdot \vec{v}\right) + S_h \quad (3)$$

being $e$ is the specific internal energy, $T$ is the temperature, and $\vec{v}$ is the velocity vector, contributing to convective transport in this equation. The specific enthalpy $h$ combines internal energy with the fluid pressure. The effective conductivity $k_{\text{eff}}$ incorporates both laminar and turbulent thermal effects. The diffusive fluxes of chemical species, represented by $\vec{J}_j$, are multiplied by the specific enthalpy $h_j$ to account for energy transport due to chemical reactions. The effective viscous stress tensor $\bar{\tau}_{\text{eff}}$ represents the internal forces associated with energy dissipation in the fluid, while $S_h$ accounts for additional volumetric energy sources, such as heat release from combustion reactions.

The filtered energy and species transport equations follow analogous forms, containing SGS flux terms for enthalpy and species mass fractions that are modeled through a gradient-transport assumption with a turbulent Prandtl number of 0.85 (Mei et al., 2022).

The SGS stress tensor is closed using the Smagorinsky-Lilly model, which computes the subgrid-scale turbulent viscosity $\mu_t$ as:

$$\mu_t = \rho L_s^2 |\bar{S}| \quad (4)$$

being $|\bar{S}| \equiv \sqrt{2\bar{S}_{ij}\bar{S}_{ij}}$ is the magnitude of the filtered strain-rate tensor, and $L_s = min(kd, C_s\Delta)$ is the characteristic length scale that blends the von Kármán mixing length near walls (with constant $\kappa = 0.41$) and the filter width $\Delta = V^{1/3}$ in the bulk flow (Johansen and Ciccarelli, 2010; Chen et al., 2016). The Smagorinsky constant was set to $C_s = 0.1$ following Lilly's calibration. Near-wall treatment was handled by the Werner-Wengle wall function, which blends linear and logarithmic profiles to correctly reproduce the asymptotic near-wall behavior across different flow regimes. The energy Prandtl number and wall Prandtl number were both set to 0.85.

The selection of LES over RANS was motivated by the demonstrated inability of RANS models to capture key physical mechanisms in confined reactive flows, including flame surface wrinkling, near-wall turbulence anisotropy, and the formation of hydrodynamic instabilities. In particular, Nguyen et al. (2021) showed that the k-ε model overpredicted flame-front velocities by up to a factor of four in geometrically similar configurations. The Smagorinsky-Lilly SGS closure was preferred over the more elaborate WALE model because it shows better performance in inhomogeneous flows with unstructured meshes, as expected in the present strongly expanding reactive environment (Nguyen et al., 2021; Chen et al., 2016).

### 2.3 Chemical Kinetics and Ignition

Hydrogen combustion was described by a one-step global reaction mechanism:

$$2H_2+(O2+3{,}76N_2) \rightarrow 2H_2O+3{,}76N_2 \quad (5)$$

Chemical kinetics were represented by a one-step global mechanism for hydrogen–air combustion:

$$\omega = A_m \rho Y exp\left(-\frac{E_{a,m}}{RT}\right) \quad (6)$$

being $\omega$ is the production rate for species $m$, $A_m$ denotes the pre-exponential factor, $\rho$is the density, $T$is the temperature, $E_{a,m}$ is the activation energy, $Y$ is the mass fraction of unburned reactant, and finally, $R$ represents the universal gas constant.

The reaction rate was computed using an Arrhenius-type expression implemented through the Finite-Rate/Eddy-Dissipation turbulence-chemistry interaction model in the ANSYS Fluent Species Transport module. This model accounts for both the intrinsic chemical kinetics and the turbulence-controlled mixing rate, adopting the minimum of the two as the effective reaction rate. The Eddy-Dissipation constants were set to A = 4.0 and B = 0.5. The Arrhenius parameters adopted in the present study are listed in Tab. 1.

Table 1. One-step Arrhenius kinetics parameters for the $H_2$/air global mechanism.

| Parameter | Value | Unit |
|---|---|---|
| Pre-exponential factor ($A_m$) | $9.87 \times 10^8$ | kmol $m^{-3}$ $s^{-1}$ |
| Temperature exponent (n) | 0 | - |
| Activation energy ($E_a$) | $3.1 \times 10^7$ | J $kmol^{-1}$ |
| Universal gas constant (R) | 8.314 | J $kmol^{-1}$ $K^{-1}$ |

The one-step mechanism, calibrated for stoichiometric conditions, was selected to limit computational cost while capturing the global heat release rate. Although more detailed multi-step mechanisms are available and would improve accuracy for off-stoichiometric conditions, they would render the computational cost prohibitive for the number of cases investigated. The implications of this simplification on the prediction of flame dynamics under the stoichiometric conditions studied here are considered acceptable for the purposes of validation and baseline characterization.

Ignition was initiated by a spark using the Spark Ignition functionality in ANSYS Fluent. The spark was placed at coordinates (0.047; 0.025; 0.000) m, consistent with the experimental configuration of Jiang et al. (2024). An ignition energy of 1 mJ was applied over a duration of 1 ms. Preliminary tests showed that variations in ignition energy within the same order of magnitude did not produce significant changes in the flame dynamics. The initial spark radius was set to 0.006 m after a systematic sensitivity study, values below this threshold did not produce the characteristic tulip flame and distorted tulip flame morphologies. The Turbulent Length flame speed model was adopted within the Spark Ignition module due to its better balance between physical accuracy and computational cost.

### 2.4 Mesh Generation

Structured hexahedral meshes were generated in the ANSYS meshing environment for the obstacle-free duct geometry. Hexahedral elements were preferred over tetrahedral elements because their cube-like shape minimizes distortion metrics, reducing numerical diffusion and improving convergence in flows with predominantly aligned gradients. A nominal element edge length of 0.74 mm was adopted, yielding approximately 1,010,344 elements for the symmetric (half-duct) domain. This choice is consistent with element sizes of 1.0 mm used by Jiang et al. (2024) and Mei et al. (2023), who demonstrated satisfactory agreement with experimental data at this resolution.

A mesh sensitivity study was conducted by comparing three refinement levels: coarse (250,000 elements; 1.17 mm edge), intermediate (500,000 elements; 0.92 mm edge), and fine (1,000,000 elements; 0.74 mm edge). The three meshes were evaluated against the experimental flame-front position and pressure time histories of Jiang et al. (2024). The fine mesh ($1 \times 10^6$ elements) provided the best agreement with experimental data and was adopted as the baseline for all subsequent simulations.

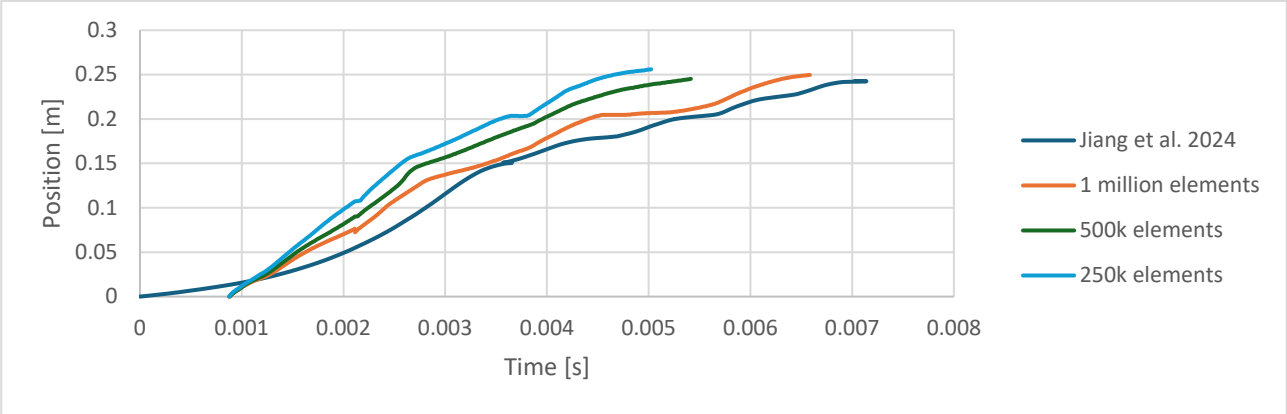


Figure 2. Mesh sensitivity: flame-front position vs. time

## 2.5 Initial and Boundary Conditions

The duct walls were treated as adiabatic, no-slip solid boundaries, consistent with the approach adopted by Xiao et al. (2014), who demonstrated that this condition adequately captures the characteristic flame morphologies in closed rectangular ducts. Radiation heat transfer was not considered in the present study.

The initial conditions imposed throughout the domain are summarized in Tab. 3. The mixture density was computed using the compressible-volume-weighted method, which ensures consistency with the compressible nature of the reactive flow. Both thermal conductivity and dynamic viscosity of the mixture were evaluated using the ideal-gas-mixing-law, as recommended by ANSYS Inc. (2021) for hydrogen-air systems under ideal-gas assumptions.

Table 2. Initial conditions for all simulations.

| Property | Value | Unit |
|---|---|---|
| Initial density ($\rho_0$) | 0.85 | kg m$^{-3}$ |
| Laminar flame speed ($S^L$) | 2.272 | m s$^{-1}$ |
| Initial temperature ($T_0$) | 300 | K |
| Initial pressure ($p_0$) | 1 | atm |
| Specific heat ratio ($\gamma$) | 1.125 | - |
| Equivalence ratio ($\Phi$) | 1.0 | - |

The simulations were run in transient mode using the First-Order Implicit time integration scheme. A time step of $\Delta t = 1.3 \times 10^{-5}$ s was adopted, and 500 time steps were computed, covering a total physical time of 6.5 ms, sufficient to capture the complete morphological evolution of the flame front and the relevant pressure dynamics. Up to 40 inner iterations were performed per time step, with convergence criteria of $10^{-6}$ for continuity, momentum, energy, and species residuals.

Spatial discretization employed a second-order scheme for pressure, Bounded Central Differencing for momentum, and second-order upwind for all scalar equations (energy and species). Gradient reconstruction used the Least-Squares Cell-Based method. A conservative Flow Courant Number of 0.1 and sub-relaxation factors of 0.1 for all transported variables were applied to ensure numerical stability in the presence of the sharp gradients associated with the reactive flame front. All simulations were performed in double-precision mode using 4 parallel CPU processes.

## 2.6 Post-Processing

Post-processing was carried out using the ParaView software. The flame-front position was extracted at each time step as the axial location of the T = 1000 K isosurface, consistent with the threshold adopted by Jiang et al. (2024). The instantaneous flame-front velocity was computed by numerical differentiation of the position-time curve. Pressure was monitored at a fixed internal probe located near the closed end of the duct at coordinates (0.047; 0.025; 0.000) m. Temperature contour maps were extracted on the duct mid-plane for qualitative morphological comparison with Schlieren images from the experimental reference.

Validation was conducted at two levels. Qualitatively, the temporal sequence of flame morphologies predicted by the model was compared with the experimental Schlieren images from Jiang et al. (2024). Quantitatively, the flame-front position as a function of time and the pressure time history at the monitoring probe were compared with the experimental measurements, providing objective metrics of model fidelity across different stages of the combustion process.

# 3. RESULTS AND DISCUSSION

### 3.1 Model Validation

Figure 3 presents the temporal sequence of flame morphologies predicted by the present LES model alongside the experimental Schlieren images of Jiang et al. (2024). The numerical results are shown as temperature contour maps on the duct mid-plane. To align the numerical results with the experimental time reference, a 0.8 ms ignition delay was applied, consistent with the differences in ignition sphere radius between the two setups. The maximum temperature recorded across all simulations was approximately 2800 K, in agreement with the expected adiabatic flame temperature for stoichiometric hydrogen-air mixtures under the simplified one-step kinetics adopted.

The numerical results reproduce the experimentally observed morphological sequence with good qualitative agreement. At early times (approximately 0.8-1.95 ms), both the experiment and the simulation show a hemispherical flame expanding from the ignition point. As the flame front interacts with the duct walls, the flame elongates preferentially in the axial direction, giving rise to the characteristic finger-shaped flame (approximately 1.95-2.95 ms). This transition is governed by the differential acceleration between the central and near-wall flame regions, driven by the no-slip boundary conditions and the volumetric expansion of combustion products.

At intermediate times (3.92-4.45 ms), the tulip flame morphology emerges in both numerical and experimental results. This shape is produced by the inversion of the flame curvature relative to the direction of propagation: reflected pressure waves from the closed end wall decelerate the central region of the flame while the near-wall portions continue to advance, ultimately reversing the convexity of the flame surface. The present LES model captures this mechanism correctly, reproducing the characteristic concave-toward-products shape of the tulip flame.

At later times (5.0-5.7 ms), both the simulation and the experiment exhibit the distorted tulip flame, characterized by additional wrinkling and asymmetries on the flame surface. These distortions arise from the combined action of three hydrodynamic instabilities: Rayleigh-Taylor instability, driven by the acceleration of the lighter burned-gas region into the heavier unburned mixture; Richtmyer-Meshkov instability, triggered by pressure pulses crossing the flame interface and generating baroclinic vorticity; and Kelvin-Helmholtz instability, arising in the shear layers that develop between adjacent flow regions. The LES framework resolves the large-scale vortical structures responsible for these instabilities explicitly, which is reflected in the close morphological agreement with the experimental images at this stage (Ciccarelli and Dorofeev, 2008).

One noteworthy discrepancy concerns the planar flame stage observed experimentally at approximately 3.7 ms, which is not reproduced by the present model. Instead, the simulation predicts an earlier onset of the tulip flame, attributed to the larger initial ignition sphere radius (0.006 m versus 0.004 m in the experiment). The planar flame morphology, which requires finer spatial and temporal resolution to be captured, was not observed in any mesh configuration tested and represents a target for future work.

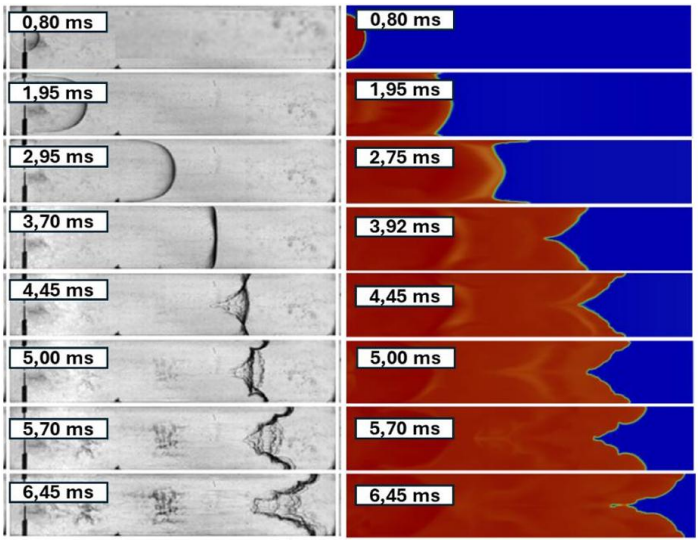


Figure 3. Comparison of experimental Schlieren images (left, from Jiang et al., 2024) and numerical temperature contour maps on the mid-plane (right) at multiple time instants covering the hemispherical, finger, tulip, and distorted tulip flame stages.

To assess the three-dimensional fidelity of the model, Fig. 4 compares temperature contour maps on the duct mid-plane and on the lateral wall plane at the tulip flame stage. Because the experimental Schlieren images capture a line-of-sight-integrated view, they simultaneously record the mid-plane tulip morphology and the near-wall wall-skirt shape. The present three-dimensional LES model reproduces this superposition. The mid-plane shows the concave tulip, while the

lateral wall plane shows the convex wall-skirt. When the two planes are overlaid, the composite closely matches the Schlieren image, confirming that three-dimensional modeling is essential for the correct representation of confined premixed flame dynamics (Emami et al., 2015).

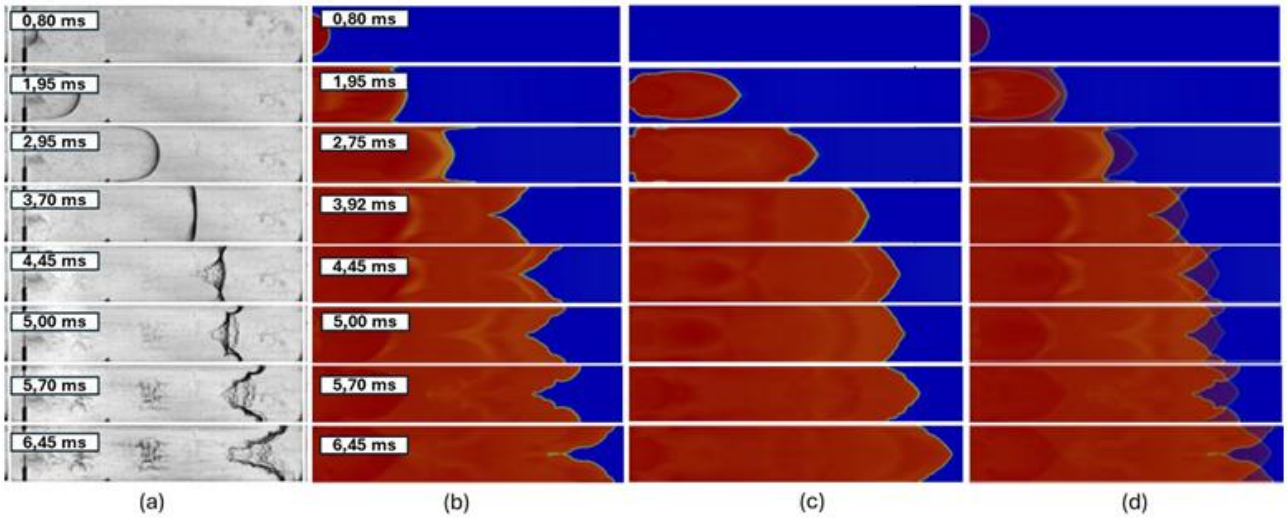


Figure 4. Mid-plane and wall-plane temperature contours at the tulip flame stage: (a) experimental Schlieren image from Jiang et al. (2024), (b) mid-plane temperature contour, (c) lateral wall-plane temperature contour, and (d) superposition of (b) and (c).

### 3.2 Quantitative Comparison: Flame-Front Position and Pressure

Figure 5 presents the flame-front position as a function of time for the present LES model and the experimental data of Jiang et al. (2024). In the early stage (0-2 ms), a discrepancy between the two curves is observed, attributed to the inability of the current mesh resolution and time step to reproduce the initial planar flame morphology, and to the larger ignition sphere radius used in the simulation, which produces a more advanced flame front at the earliest instants.

As the combustion evolves, the agreement progressively improves. In the intermediate and late stages (approximately 2.5-6.5 ms), the numerical and experimental curves converge, exhibiting consistent propagation rates. This result demonstrates that the model accurately captures the flame acceleration dynamics once the early ignition-related transient becomes less dominant, and confirms the adequacy of the fine mesh (1 x $10^6$ elements) adopted following the sensitivity analysis.

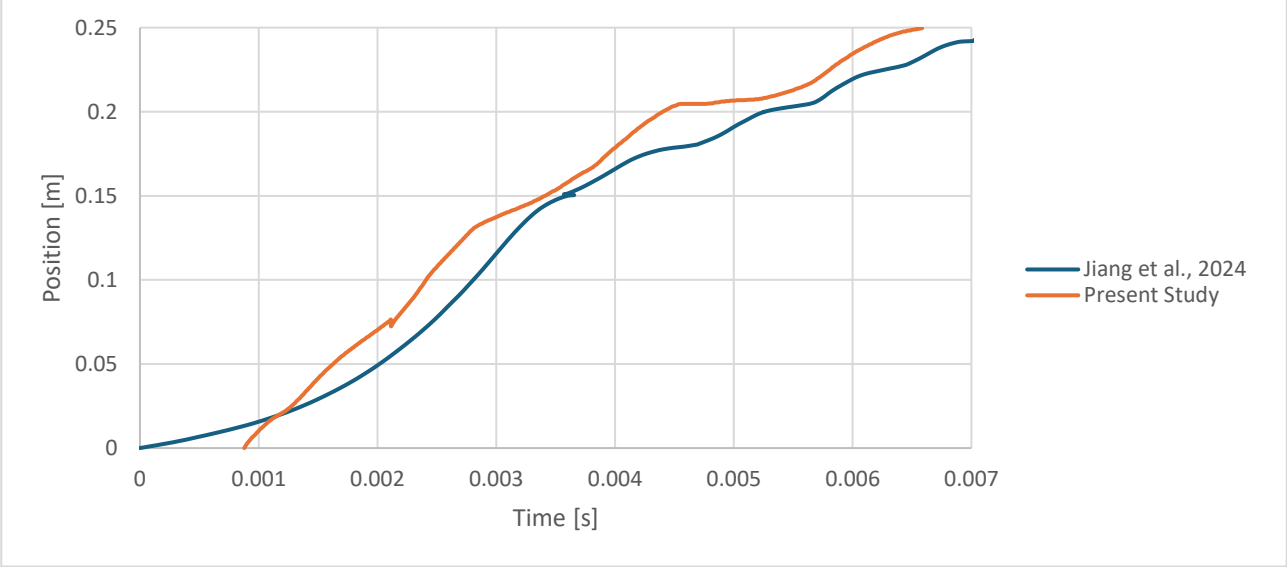


Figure 5. Flame-front position vs. time: numerical vs. experimental

Figure 6 shows the pressure time history at the fixed monitoring probe located at coordinates (0.047; 0.025; 0.000) m. The numerical pressure profile reproduces the general growth trend observed experimentally, with multiple successive peaks of increasing amplitude associated with the progressive intensification of turbulent combustion. In the early instants, the simulation anticipates the pressure rise slightly relative to the experiment, consistent with the earlier flame-front advancement discussed above. In the intermediate range (4.0-5.0 ms), partial overlap of the pressure peaks is achieved. In the late stage (after 6.0 ms), the numerical model slightly underpredicts the peak pressure magnitudes, with a maximum difference of approximately 57 kPa at 7 ms. This underprediction is attributed to the finite mesh resolution limiting the representation of small-scale turbulent structures that contribute to the pressure amplification. Despite this, the oscillation frequency and the overall growth trend are correctly captured throughout the simulation.

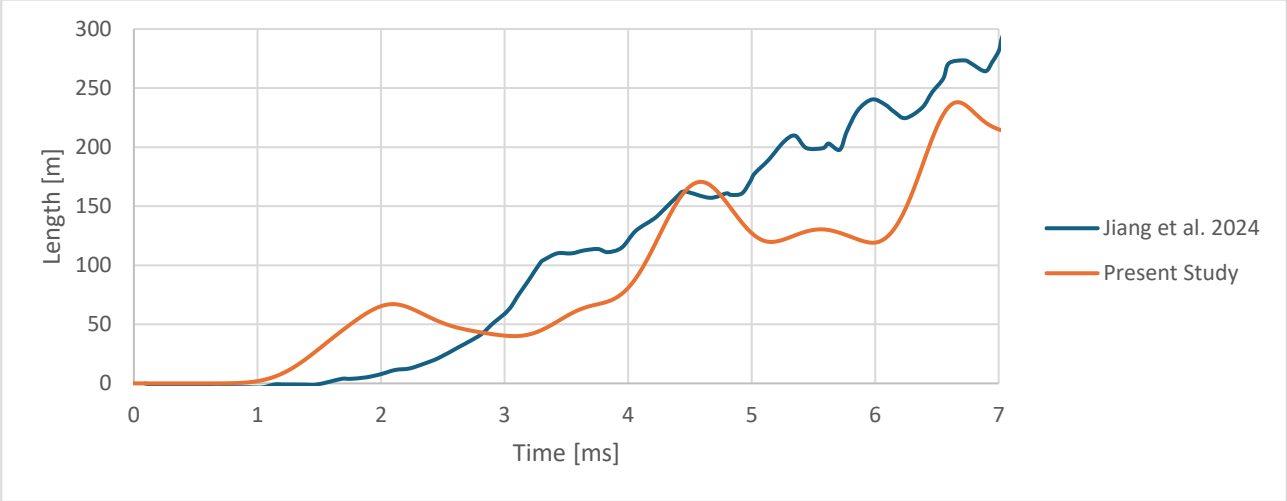


Figure 6. Pressure vs. time at the monitoring probe: numerical vs. experimental

## 4. CONCLUSIONS

This work presented the development and validation of a three-dimensional LES model for premixed hydrogen-air flame propagation in a closed rectangular duct without obstacles. The Smagorinsky-Lilly subgrid-scale closure implemented in ANSYS Fluent, combined with a one-step global Arrhenius kinetics mechanism and a structured hexahedral mesh of approximately 1 x $10^6$ elements, was shown to reproduce the characteristic flame morphological sequence hemispherical, finger-shaped, tulip, and distorted tulip flames, in qualitative agreement with the experimental Schlieren images of Jiang et al. (2024). The three-dimensional character of the simulation was demonstrated to be essential for capturing the simultaneous mid-plane and near-wall flame dynamics observed in the experimental Schlieren images.

Quantitatively, satisfactory agreement was achieved for the flame-front position and pressure time histories in the intermediate and late stages of propagation, validating the predictive capability of the model for the relevant combustion dynamics. Discrepancies in the early stage, including the absence of the planar flame morphology, are attributed to finite mesh resolution, to the larger ignition sphere radius required to trigger the characteristic flame shapes at the current refinement level, and to the use of a simplified one-step mechanism based on the Arrhenius equation. These limitations represent clear targets for improvement in future work through finer spatial discretization in the ignition region, reduced time steps, and more detailed chemical kinetics modeling.

The validated computational framework constitutes a robust baseline for future investigations of obstacle-induced flame acceleration in hydrogen-air systems, with direct implications for risk assessment in hydrogen infrastructure and for the design of controlled combustion devices operating in confined geometries.

## 5. ACKNOWLEDGEMENTS

This work has been partially funded by the Brazilian agencys CAPES and CNPq.

## 6. REFERENCES

ANSYS Inc., ANSYS Fluent Theory Guide, Release 2021 R1. ANSYS Inc., Canonsburg, PA, 2021.

Chen, Z., Fan, B., Ye, S. and Zheng, K., "Effect of step obstacles on premixed flame propagation in a closed rectangular duct", Combustion Science and Technology, Vol. 188, pp. 1187–1202, 2016.

Ciccarelli, G. and Dorofeev, S., "Flame acceleration and transition to detonation in ducts", Progress in Energy and Combustion Science, Vol. 34, No. 4, pp. 499–550, 2008.

Emami, S., Mazaheri, K., Shamooni, A. and Mahmoudi, Y., "LES of flame acceleration and DDT in hydrogen-air mixture using artificially thickened flame approach and detailed chemical kinetics", International Journal of Hydrogen Energy, Vol. 40, pp. 7395–7408, 2015.

Fan, J., Zhang, X., Xiao, H., Hu, L., Wang, L., Ma, H. and Qin, X., "Three- versus two-dimensional numerical simulation of distorted tulip flame in stoichiometric hydrogen-air mixture", Combustion and Flame, Vol. 285, 114733, 2026.

Jiang, X., Li, X., Zhao, Y. and Sun, Z., "Experimental and numerical investigation of premixed hydrogen-air flame propagation in a closed rectangular duct", Combustion and Flame, Vol. 259, 2024.

Johansen, C. T. and Ciccarelli, G., "Visualization of the unburned gas flow field ahead of an accelerating flame in an obstructed square channel", Combustion and Flame, Vol. 157, pp. 1850–1861, 2010.

Karanam, A., Sharma, P. K. and Ganju, S., "Numerical simulation and validation of flame acceleration and DDT in hydrogen air mixtures", International Journal of Hydrogen Energy, Vol. 43, pp. 17492–17504, 2018.

Lei, B., Guo, Z. and Zhao, Z., "Study of the influence of flame instability on tulip flame formation", International Journal of Hydrogen Energy, Vol. 99, pp. 418–428, 2025.

Mei, Z., Zhao, J., Lv, H. and Wang, J., "Large eddy simulation of premixed hydrogen/air flame propagation in a closed curved duct", International Journal of Hydrogen Energy, Vol. 47, pp. 37922–37934, 2022.

Mei, Z., Zhao, J., Lv, H. and Wang, J., "Effects of obstacle arrangements on premixed $H_2$/air flame propagation in an obstructed rectangular duct", Fuel, Vol. 344, 2023.

Nguyen, T., Strebinger, C., Bogin Jr., G. E. and Brune, J., "A 2D CFD model investigation of the impact of obstacles and turbulence model on methane flame propagation", Process Safety and Environmental Protection, Vol. 146, pp. 95–107, 2021.

Sheng, Z., Yang, G., Gao, W., Li, S., Shen, Q. and Sun, H., "Study on the dynamic process of premixed hydrogen-air deflagration flame propagating in a closed space with obstacles", Fuel, Vol. 334, 126542, 2023.

Turns, S. R., An Introduction to Combustion: Concepts and Applications, 3rd ed., McGraw-Hill, New York, 2013.

Versteeg, H. K. and Malalasekera, W., An Introduction to Computational Fluid Dynamics: The Finite Volume Method, 2nd ed., Pearson Education, 2007.

Wang, J., Zhao, X., Gao, L., Wang, X. and Zhu, Y., "Effect of solid obstacle distribution on flame acceleration and DDT in obstructed channels filled with hydrogen-air mixture", International Journal of Hydrogen Energy, Vol. 47, pp. 12759–12770, 2022.

Xiao, H., Sun, J. and Chen, P., "Experimental and numerical study of premixed hydrogen/air flame propagating in a combustion chamber", Journal of Hazardous Materials, Vol. 268, pp. 132–139, 2014.

## 7. RESPONSIBILITY NOTICE

The authors are responsible for the printed material included in this paper.